Melting of magnetic order in $NaOsO_3$ by femtosecond laser pulses

Flavio Giorgianni,[1,*] Max Burian,[1] Namrata Gurung,[1,2] Martin Kubli,[1,3] Vincent Esposito,[1] Urs Staub,[1] Paul Beaud,[1] Steven L. Johnson,[1,3] Yoav William Windsor,[1,4] Laurenz Rettig,[1,4] Dmitry Ozerov,[1] Henrik Lemke,[1] Susmita Saha,[1,2,5] Federico Pressacco,[6,7] Stephen Patrick Collins,[8] Tadashi Togashi,[9,10] Tetsuo Katayama,[9,10] Shigeki Owada,[9,10] Makina Yabashi,[9,10] Kazunari Yamaura,[11] Yoshikazu Tanaka,[10] and V. Scagnoli[1,2,†]

[1]*Paul Scherrer Institute, 5232 Villigen PSI, Switzerland*
[2]*Laboratory for Mesoscopic Systems, Department of Materials, ETH Zurich, 8093 Zurich, Switzerland*
[3]*Institute for Quantum Electronics, Physics Department, ETH Zurich, 8093 Zurich, Switzerland*
[4]*Fritz Haber Institute of the Max Planck Society, Faradayweg 4-6, 14195 Berlin, Germany*
[5]*Department of Physics and Astronomy, Uppsala University, 751 21 Uppsala, Sweden*
[6]*Physics Department and Centre for Free-Electron Laser Science (CFEL), University of Hamburg, 22761 Hamburg, Germany*
[7]*The Hamburg Centre for Ultrafast Imaging (CUI), 22761 Hamburg, Germany*
[8]*Diamond Light Source, Harwell Science and Innovation Campus, Didcot, Oxfordshire OX11 0DE, United Kingdom*
[9]*Japan Synchrotron Radiation Research Institute (JASRI), 1-1-1 Kouto, Sayo-cho, Sayo-gun, Hyogo 679-5198, Japan*
[10]*RIKEN SPring-8 Center, 1-1-1 Kouto, Sayo-cho, Sayo-gun, Hyogo 679-5148, Japan*
[11]*International Center for Materials Nanoarchitectonics (WPI-MANA), National Institute for Materials Science, Namiki 1-1, Tsukuba, Ibaraki 305-0044, Japan*

(Received 5 October 2021; revised 31 March 2022; accepted 5 April 2022; published 22 April 2022)

$NaOsO_3$ has recently attracted significant attention for the strong coupling between its electronic band structure and magnetic ordering. Here, we used time-resolved magnetic x-ray diffraction to determine the timescale of the photoinduced antiferromagnetic dynamics in $NaOsO_3$. Our measurements are consistent with a sub-100 fs melting of the antiferromagnetic long-range order that occurs significantly faster than the lattice dynamics as monitored by the transient change in intensity of selected Bragg structural reflections, which instead show a decrease of intensity on a timescale of several ps.

DOI: 10.1103/PhysRevB.105.155147

I. INTRODUCTION

The discovery of sub-ps demagnetization in ferromagnets upon ultrafast laser excitation [1] has triggered an intense wave of research focusing on understanding the fundamental mechanisms involved in the dissipation of the spin and orbital angular momenta [2–7]. This fundamental research interest in the ultrafast manipulation of magnetic order is complemented by its potential applications for high-speed data storage and processing technologies, as well as its relevance for faster spintronic architectures; where, for example, one major goal of research on these systems is to develop ultrafast methods of switching between metastable magnetic states [8–13].

Recent research efforts within ultrafast magnetism have been partly focused on antiferromagnets [14–18] since they possess resonant frequencies in the terahertz (THz) range, which is three orders of magnitude higher than observed for ferromagnets (see Ref. [19] and references therein). Furthermore, in these systems the angular momentum can be directly exchanged between the spin-up and spin-down magnetic sublattices. Having equivalent stable states with zero net angular momentum in the spin system, antiferromagnets are expected to exhibit faster dynamics, different from those observed in ferromagnets, where momentum transfer to the lattice occurs. Given the ubiquity of antiferromagnetic materials, they offer a rich playground for investigating ultrafast spin dynamics. Of particular interest is the fact that in the majority of antiferromagnetic systems, the magnetic ordering is intimately related to the electronic structure of the material. Therefore, by manipulating the electronic structure, one also affects the antiferromagnetic order parameter. Indeed, theoretical predictions [20–22] suggest that in antiferromagnetic materials falling in the weak and strong electron coupling regime, quenching of the antiferromagnetic order parameter occurs concomitantly within the photoexcited dynamics of the electronic system, which implies few-fs or faster timescales are possible. Laser-induced ultrafast reorientation or switching of the antiferromagnetic order parameter has been demonstrated in several materials [19,23–30], including Mott insulators [25,27,28]. However, there have been a limited amount of reports that discuss the ultimate timescale of the antiferromagnetic quenching in strongly correlated systems following an ultrafast photoexcitation [27,31–34]. In these reports, the timescales have been limited either by the experimental time resolution or found to be in the 100–400 fs range, which is significantly slower when compared with the values predicted theoretically [20–22] or reported for ferromagnetic materials and multilayer films [1,35–39]. It is therefore interesting to

*flavio.giorgianni@psi.ch
†valerio.scagnoli@psi.ch

ascertain on which timescales the electronic and magnetic properties can be modified, in particular, in systems in which antiferromagnetic order occurs concomitantly with an abrupt change in the electronic properties of the material, as occurring at an insulator-to-metal transition.

In this paper, we report the ultrafast manipulation of the antiferromagnetic order and the electronic structure in $NaOsO_3$. The photoexcitation of $NaOsO_3$ by femtosecond laser pulses with photon energy above the insulating gap simultaneously drives the dynamics of electrons and spins. To uniquely access the laser-induced ultrafast spin dynamics we use time-resolved femtosecond x-ray diffraction on a magnetic Bragg peak. Our results show that the manipulation of the antiferromagnetic order parameter occurs on a sub-100 fs timescale.

$NaOsO_3$ undergoes an insulator-to-metal transition concomitant with antiferromagnetic ordering at $T_{\rm IM} = T_N = 410(1)$ K [40]. In this compound, the absence of crystallographic symmetry breaking [41,42] is suggestive of a magnetically driven insulator-to-metal transition. However, due to the presence of energetically similar competing interactions, a consensus on the nature of the metal-insulator mechanism operating in this perovskite is absent [41–46]. In the insulating phase, with a gap at low temperature of 102(3) meV [47], the magnetic moment determined by neutron diffraction refinement is 1 μ_B, and it suggests a coexistence of localized and itinerant magnetism [41]. Below $T_{\rm N}$, magnetic moments order almost parallel to the c axis in a G-type antiferromagnet with a very small ($<0.01\,\mu_{\rm B}$) ferromagnetic component along the b axis (*Pnma*). The strong enhancement of magnetic diffraction at the Os L_3 edge (10.787 keV) makes this material very appealing for time-resolved x-ray diffraction measurements of the antiferromagnetic dynamics. The latter can be related to the changes in the conductivity response of the material upon fs laser excitation, which are expected to drive an insulator-to-metal transitioning the system.

This paper is organized as follows: In Sec. II, we describe the sample preparation and the experimental details of the pump-probe experiments. In Sec. III, we present the experimental results describing the antiferromagnetic dynamics in a time window of a few ps subsequent to a sub-100 fs laser excitation. These results are analyzed with a time-dependent order parameter model that was applied previously to manganite materials [48]. We find that the melting of the antiferromagnetic order following a fs laser excitation occurs on a timescale comparable with the experimental time resolution and faster compared to other 5d oxide materials. Lattice dynamics, monitored via the transient change of the intensity of structural Bragg peaks, occur on a timescale of several ps.

II. EXPERIMENTAL DETAILS

The resonant x-ray diffraction experiment was carried out at the EH2 end station of the BL3 beamline at the SACLA x-ray free electron laser [49], using a Huber four-circle ($2\theta, \theta, \chi$, and ϕ) diffractometer in horizontal scattering geometry equipped with a single module multiport charged coupled device detector [50]. An illustration of the experimental setup is shown in Fig. 1. In the experiment, a $NaOsO_3$ single-crystal sample with a surface normal direction close to [1 0 0] and an

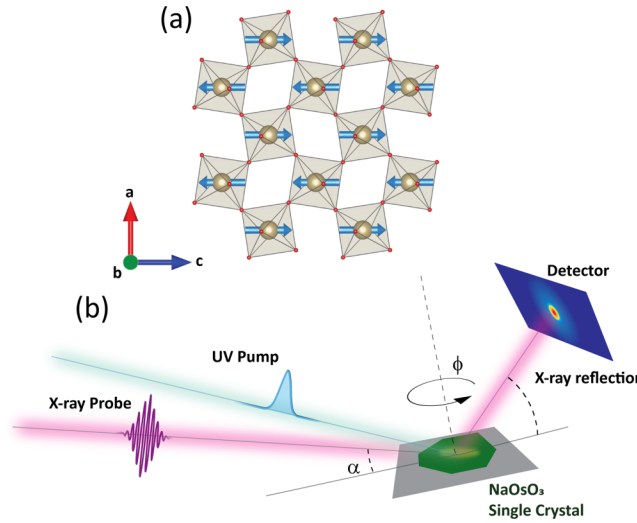

FIG. 1. Time-resolved resonant x-ray diffraction experiment. (a) Antiferromagnetic order of $NaOsO_3$ for $T < T_N$ in the a, c plane. The Os magnetic moments (blue arrow) lying along the c axis. The OsO_6 octahedral cages are colored in grey, with oxygen atoms represented in red. (b) Schematic setup of the optical-pump/x-ray-probe experiment. The experiment was performed in grazing incidence geometry $\alpha < 1$ deg and with the UV pump laser (400 nm) at an angle of 7° with the x rays. The angle α is the angle between the incident x rays and the sample surface. The angle ϕ rotates the sample about its surface normal.

area of $\sim 100 \times 100\,\mu{\rm m}^2$ was mounted on a goniometer with a nitrogen cryostream to stabilize the temperature at approximately 293 K. A $\hat{\tau}_L = 65$ fs full width at the half maximum (FWHM) optical pulse with wavelength 400 nm excited the sample with a repetition rate of 60 Hz. The laser spot size at the sample position was measured to be $300\,\mu{\rm m} \times 300\,\mu{\rm m}$. The horizontal polarized x-ray beam operating at 30 Hz and with a pulse duration of $\hat{\tau}_X = 10$ fs (FWHM) was focused to a spot size of $10\,\mu{\rm m} \times 10\,\mu{\rm m}$. During the experiment, the angle between the incoming x ray and laser beams was kept fixed at 7°, with the UV laser beam and the incoming x rays both contained in a plane perpendicular to the one defined by the incoming and diffracted x rays. An x-ray grazing incidence geometry ($\alpha = 0.5^\circ$) was used to match the x-ray and laser penetration lengths, with the latter estimated to be 50 nm from Ref. [47] for a powder sample. Independent shutters for the laser and x-ray beams were used to collect data with and without laser excitation.

The x-ray beam energy was tuned within the vicinity of the Os L_3 edge ($2p - 5d$ transition) at around 10.787 keV ($\lambda = 0.115$ nm). The temporal jitter between x-ray and optical laser pulses was measured shot-by-shot using a transmission grating based timing tool, which has an accuracy $\Delta t_{TT} = 10$ fs (FWHM) [51]. The temporal fingerprint of each shot was then used to rebin all data into $\Delta t_{\rm bin} = 50$ fs time segments [52]. The effective time resolution of the experiment was estimated to be $\Delta t_{\rm eff} = \sqrt{\hat{\tau}_L^2 + \hat{\tau}_X^2 + \Delta t_{TT}^2 + \Delta t_{\rm bin}^2} = 83(5)$ fs (FWHM). As is customary to model time traces using an $\mathrm{erf}(t/\tau)$ function [53,54], which is characterized by a timescale τ which

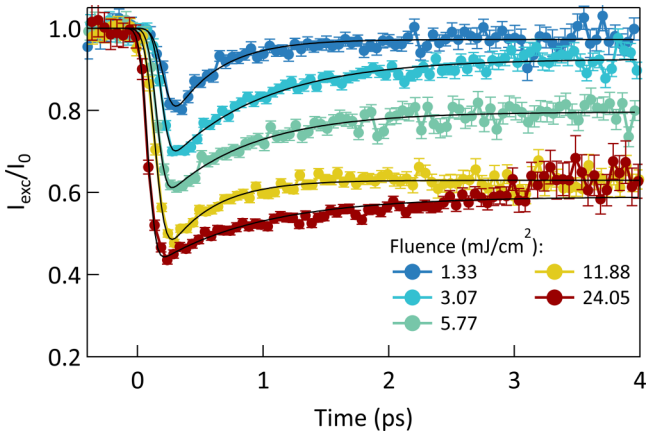

FIG. 2. Normalized diffraction intensity changes of the (1 $\bar{5}$ 0) magnetic reflection at the Os L_3 edge for several laser fluence at T = 293 K. Error bars reflect the standard deviation of the data within each bin. Solid lines are fit to the data obtained with Eq. (1).

is different from the timescale $\hat{\tau}$ expressed in terms of the FWHM, the experimental time resolution τ_{eff} can also be expressed as $\tau_{\text{eff}} = \Delta t_{\text{eff}}/\sqrt{4\ln(2)} = 51(4)$ fs.

III. RESULTS AND MODELLING

To monitor the time evolution of the antiferromagnetic order parameter in response to an ultrafast laser excitation, we have taken advantage of the enhancement of the x-ray magnetic cross section in the vicinity of the Os L_3 edge. Based on the experimental geometric constraints, we have selected the (1 $\bar{5}$ 0) magnetic reflection as the most suitable one with which to perform our pump-probe measurements. The time evolution of the (1 $\bar{5}$ 0) peak maximum intensity upon optical laser excitation is illustrated in Fig. 2 for several laser excitation fluences. In all of the time traces, a sudden decrease of intensity is observed within 100 fs after the optical laser excitation. Angular ϕ scans (rocking curves) at fixed time delay (see Fig. 5) confirm that the magnetic peak position in reciprocal space does not change within the first 10 ps after excitation. Therefore, we observe a reduction of the diffracted intensity related to the reduction of the sublattice magnetization up to 60% on a sub-ps timescale, followed by a recovery of the intensity on a several ps timescale. The persistence of a sizable part of the magnetic diffraction intensity is likely due to the imperfect matching of the laser and the x-ray penetration depths in a crystal as observed, for example, in similar experiments [33,55,56].

To extract an upper bound for the relevant timescales from these time traces and to readily compare such values with other experimental results [31–34], we have fit the data using an error function, which captures the fast decay time (τ), multiplied by an exponential term that captures the recovery time (τ_{rec}). This model is appropriate when the response of the material to the excitation is linear and significantly faster than the time resolution of the experiment, which in this case is determined by the pump and probe pulse duration as well as their relative timing stability. The fitting function has the following analytical form:

$$f(t) = \frac{1}{2}\left[\text{erf}\left(\frac{t-t_0}{\tau}\right) + 1\right] \times [A\, e^{-(t-t_0)/\tau_{\text{rec}}} + c], \qquad (1)$$

where A and c are fit parameters that represent, respectively, the amplitudes of the intensity reduction and the long-lived transient, which lasts well beyond the 4 ps time window. Here, t_0 represents the time where the x rays and the optical laser impinge concomitantly on the sample. To reproduce accurately the time traces, we have found that t_0 must be treated as a fit parameter. The shift in t_0 we observe as a function of the excitation laser fluence is possibly due to an uncontrolled drift of t_0 during the experiment or to saturation effects. The latter would lead also to a change in τ as a function of fluence, that we do not observe outside experimental uncertainties.

TABLE I. Parameters obtained by fitting the experimental data for the magnetic (1 $\bar{5}$ 0) reflection with Eq. (1). Numbers within brackets represent standard deviations. F stands for fluence.

F (mJ/cm^2)	t_0 (fs)	τ (fs)	A	τ_{rec} (ps)	c
1.33	132(8)	69(9)	–0.11(6)	0.54(5)	–0.001(3)
3.07	133(4)	69(7)	–0.13(3)	0.71(6)	–0.034(4)
5.77	85(3)	78(11)	–0.12(5)	0.71(7)	–0.099(4)
11.88	74(3)	75(4)	–0.10(5)	0.47(5)	–0.180(5)
24.05	72(2)	63(5)	–0.09(5)	0.66(4)	–0.207(3)

Taking into account the caveats above, we observe that the fit of a time trace returns a value of τ on the order of 65–75 fs for the fast decay constant (see Table I). Therefore, our experiments reveal the presence of a sub-100 fs drop of the magnetic peak intensity, for all the laser fluences, with an average decay time $\tau = \tau_{\text{AFM}} = 71 \pm 6$ fs. In addition, we observe two distinct behaviors as a function of the laser fluence. For fluences below 5 mJ/cm^2, the antiferromagnetic ordering recovers almost completely to the initial intensity with the first 2–3 ps, while for higher laser fluences the intensity remains suppressed over the time window of our measurements. A similar behavior has been observed in other transition metal based oxide materials [32,57–61] and is often assumed to herald the occurrence of a phase transition in the probed sample volume. To obtain a more quantitative description of our measurements, we apply a modified version of the model presented in Refs. [48,62,63] based on an effective time-dependent order-parameter η, which in our case represents the staggered magnetization associated with the antiferromagnetic ordering.

Within this model, there exists a threshold value n_c of the absorbed local energy density per volume n above which the system undergoes a phase transition where the order parameter vanishes. In our case, this will correspond to the melting of the long-range antiferromagnetic order when the ratio $n/n_c > 1$, i.e., when the sublattice magnetization vanishes. The time-dependent order-parameter model can take into account the effective time resolution of the experiment Δt_{eff} and the fact that the optical laser pulses are absorbed as they propagate through the sample.

Specifically, we account for the depth-dependent excitation profile by splitting the sample into $N = 400$ layers of thickness

of $\Delta z = 1$ nm. The electronic excitation density n_i of a layer at a depth z_i is then $n_{0i} = n_0\, e^{-z_i/z_L}$, where z_L is the effective laser penetration depth. For a given laser fluence F, $n_0 = F/z_L$. As explained in detail in Appendix A, we express the diffracted intensity $I_{\rm exc}(t)$ as

$$I_{\rm exc}(t)/I_0 \propto \sum_{i=0}^{N} |\eta(z_i, t)|^2, \tag{2}$$

where $\eta(z_i, t)$ is the time-dependent order parameter normalized to unity at time before excitation and for times during and after the excitation given by

$$\eta(z_i, t) = \left(1 - \frac{\min(n(z_i, t), n_c)}{n_c}\right)^{\gamma_0}, \tag{3}$$

where n_c is a critical excitation density and $n(z_i, t)$ is the absorbed local energy density per volume, which depends on the incoming pump fluence F and γ_0 is analogous to a critical exponent of the initial excitation. If $n(z_i, t) > n_c$, the phase transition to the paramagnetic state occurs and $\eta = 0$. To account for the recovery of the order parameter, an energy dissipation term is introduced in the expression for $n(z_i, t)$ [48],

$$n(z_i, t) = (n_0(z_i, t) - \alpha n_c) e^{-\frac{t}{\tau_{\rm rec}}} + \alpha n_c, \tag{4}$$

In using this form for $n(z_i, t)$ we approximate the relaxation of the electronic energy density as a two-step process. The time constant $\tau_{\rm rec}$ characterizes a fast relaxation via electron-phonon interactions, which is followed by a much slower relaxation characterized by a time constant much larger than the measurement time window. Here [48,61]

$$\alpha = 1 - \left(1 - \frac{n_0(z_i, t)}{n_c}\right)^{\frac{\gamma}{\gamma_0}}, \tag{5}$$

where γ is an effective critical exponent of the quasithermalized system after the initial relaxation process.

The quantity α is a function of γ_0 and γ, which can be regarded as the critical exponents with respect to the initial excitation ($t \approx 0$) and after equilibration ($t \gg \tau_{\rm rec}$). If $\gamma_0 = \gamma$, $\alpha = n_0(z_i, t)/n_c$ and the variation in the observed intensity will be the same at short and large times after the laser excitation. If $\gamma_0 > \gamma$, the change in the measured intensity will be larger at the shorter timescales, signaling the presence of a mechanism leading to a partial recovery of the order parameter with a time constant $\tau_{\rm rec}$. For $\gamma_0 \gg \gamma$, one could anticipate an almost complete recovery of the order parameter, at least for the lowest excitation fluences.

We assume for the initial electron energy density

$$n_0(z_i, t)dz = \frac{F}{2}\left(1 - e^{-\frac{dz}{z_L}}\right) e^{-\frac{z_i}{z_L}} \left[1 + \mathrm{erf}\left(\frac{t}{\tau_L + \hat{\tau}}\right)\right], \tag{6}$$

which describes the energy deposited by the pump laser pulse of duration τ_L at a given depth z_i. With such a model, we are able to describe reasonably well all the observed time traces, as shown in Fig. 3. From the simultaneous fit of all the time traces, we find the following values (and associated uncertainties) for the fit parameters: the effective optical penetration depth $z_L = 20.9(8)$ nm, which is reasonable if we consider that the effective optical penetration depth is reduced in our

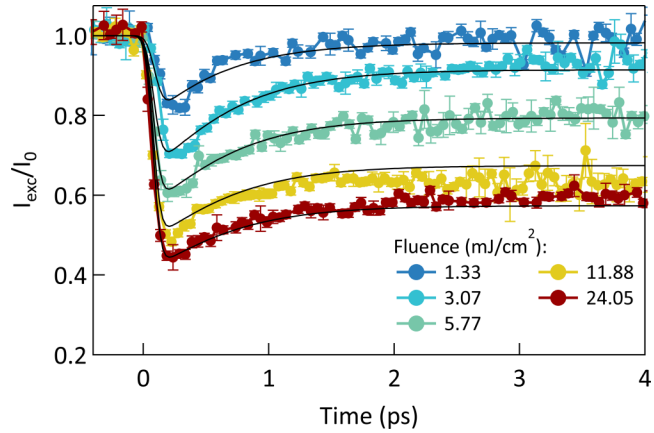

FIG. 3. Fits to the time-dependent magnetic reflection data using the time-dependent order parameter model described in the text for different laser pump fluences.

geometry when compared to the 50-nm value estimated for a powder sample in normal incidence conditions [47]. The critical excitation density is $n_c = 813(3)\,\mathrm{J/cm^3}$ and the critical exponent is $\gamma_0 = 1.28(7)$, which is considerably higher than the values 0.5 and 0.69(3) reported for $PrCaMnO_3$ [48] and for $PrCaMnO_4$ [61], respectively. The estimated value for the γ_0 exponent in this experiment suggests an approximately quadratic relation between the scattering intensity and the excitation energy density. The value of $\gamma = 0.08(1)$ is smaller than that reported for $PrCaMnO_3$ [48] and $PrCaMnO_4$ [61], where it was found $\gamma = 0.20(1)$ and $\gamma = 0.29(3)$, respectively. The differences between the fitted values of both γ and γ_0 for the present experiment and these previous studies may be partially due to the fact that the previous studies were on thin films, whereas the current study is on a bulk sample where the laser excitation depth is smaller than the x-ray penetration depth. Since the model does not explicitly treat energy transport effects, the fitted values of the parameters may be influenced by these effects. Nevertheless, the ratio of γ/γ_0 is significantly smaller for $NaOsO_3$, making it plausible to conclude that the electronic energy dissipation term is more effective in $NaOsO_3$ as characterized by a relaxation constant $\tau = 0.48(3)$ ps, whereas in $PrCaMnO_3$ it was $\tau = 0.81$ ps. Such results could possibly reflect the difference in the phase transition occurring in those two classes of materials, with the manganites undergoing a change in the structure of the material, while this should not be the case for $NaOsO_3$ [41]. In such a scenario, one would expect a recovery requiring a lattice rearrangement to occur on a longer timescale than a reordering of spins to their antiferromagnetic ground state ordering. The observed recovery timescale $\tau_{\rm rec}$ points to the presence of an efficient thermalization process of the transient-free carrier population induced by the pump pulse, consistent with the small gap and the partially delocalized nature of the magnetism in $NaOsO_3$.

Finally, the model, taking into account the experimental resolution, enables us to extract the melting timescale of the antiferromagnetic order, estimated in $\hat{\tau} = 62(12)$ fs. The resulting timescale of the melting of the antiferromagnetic order following a fs laser excitation is faster compared to other $5d$ oxide materials [32,33,64] (see Table II) and, in agreement

TABLE II. This table illustrates the decay constants τ_m and τ_e, determined by Eq. (1), associated with the magnetic and electronic degree of freedom, respectively. Selected oxides compounds, whose timescale of the melting of the antiferromagnetic phase has been reported, are included. T_m (K) indicates the temperature at which the pump-probe experiments on the antiferromagnetic order parameter were performed. The ratio T_m/T_N is also reported, as it could affect the measured value of τ_m.

Sample	τ_m (fs)	τ_e (fs)	T_m (K)	T_m/T_N	Reference
$Sr_3Ir_2O_7$	<120[a]	<95[a]	110	0.39	[33,70]
Sr_2IrO_4	330	250	75	0.39[b]	[32]
Sr_2IrO_4	560	250	190	0.97[b]	[32]
$NdNiO_3$	<125[a]	<60[a]	40	0.27	[34,71]
$NaOsO_3$	71(6)	<90[a]	300	0.73	this paper

[a]Limited by experimental time resolution.
[b]For the thin film sample used in Ref. [32] $T_N \sim 195$ K.

with the estimate based on Eq. (1), and is comparable with the experimental resolution. The critical behavior of the squared order parameter η^2 as a function of the excitation fluence is illustrated in Fig. 4, which compares the measured relative changes of the scattering intensity at 0.2–0.3 ps and 2.2–3 ps after later laser excitation. The fluence $F_c = 2.5(2)\,\mathrm{mJ/cm^2}$ corresponding to the critical value of the energy density n_c at the surface has a value similar to that observed in the manganites [48,61] and for the melting of the charge ordering in $NdNiO_3$ [62], which has also an insulator-to-metal transitioncoinciding with antiferromagnetic ordering. The photoinduced magnetic response in the nickelate shows as for $NaOsO_3$ a prompt recovery of the magnetic ordering for low laser fluences ($<1\ \mathrm{mJ/cm^2}$), suggesting that the critical fluence for this nickelate is lower than for $NaOsO_3$. However, one should exercise caution in comparing fluence values from different experiments as they strongly rely on values of laser power and beam size measurements that can be affected by significant uncertainties.

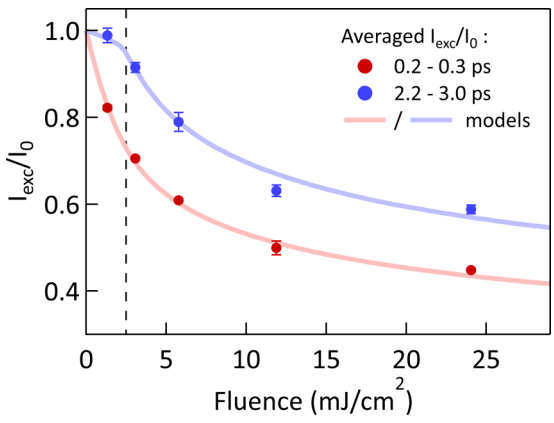

FIG. 4. Absorbed fluence dependence of the normalized intensity at 0.25 ps and at 2.65 ps. Error bars represent the standard deviation of the measurement points gathered in the vicinity of the nominal value for each fluence. The dashed line specifies the fluence corresponding to the critical energy density at the surface. Solid lines are obtained by using the model described in the text.

IV. DISCUSSION

There is a consistent body of evidence that impulsive laser excitations above the band gap are able to drive an insulator-to-metal transition [65–68] and, for samples which concomitantly order antiferromagnetically, destroy the antiferromagnetic long-range ordering [31–34,64]. In these materials, one expects to be able to use time-resolved experiments to draw conclusions on the hierarchy of interactions leading to the development of the insulator-to-metal transition. Specifically, it is interesting to see if the insulator-to-metal transitioning oxides based on transition metal atoms could be categorized following the observed changes in physical properties in response to impulsive laser excitation. For example, $NaOsO_3$ originally attracted interest, as it was thought to be a rare example of a Slater insulator [41,42], namely, showing a magnetically driven insulator-to-metal transition. While alternative explanations of the nature of the insulator-to-metal transition have been proposed [44–46], it is clear that there is a strong coupling between the magnetism and electronic structure [41–44].

It would therefore be interesting to compare the sub-100 fs dynamics in $NaOsO_3$ with those of $NdNiO_3$ in which there is a large consensus on the fact that the appearance of the antiferromagnetic phase is a byproduct of the concurrent insulator-to-metal transition. $NdNiO_3$ is a charge transfer insulator (a Mott insulator has a gap between two bands of the same character, e.g., both $3d$, whereas for a charge transfer insulator the gap has a mixed character, e.g., between the oxygen $2p$ and the transition-metal $3d$ bands) and one would expect the electronic response time τ_e to be faster than τ_m, the magnetic one. Vice versa, for $NaOsO_3$ one would expect τ_m to be comparable with τ_e. In this respect, neither our data nor those presented in Refs. [31,34] are conclusive as they are limited by time resolution available in the time-resolved x-ray measurements. Our experiments on $NaOsO_3$ have shown that the magnetic response to a fs optical excitation occurs within a few tenths of fs after the fs laser excitation. Modeling the time trace with Eq. (1) gives $\tau_m \sim 71(6)$ fs, while the model described in Sec. III, which takes into account the experimental time resolution, gives $\tau_m \sim 62(12)$ fs. These values are comparable with those of τ_e in $NaOsO_3$ and $NdNiO_3$, which are also limited by the time resolution of the optical experiments (see Table II). While from our measurements at room temperature it would be tempting to conclude that $\tau_m > \tau_e$, it must be noted that the magnetization time response τ_m in antiferromagnetic Sr_2IrO_4 can be halved when experiments are conducted at low temperatures T_m sufficiently far from T_N [32].

Regrettably, drawing conclusions on the microscopic parameters governing the timescale of the disappearance of the antiferromagnetic order parameter upon impulsive laser excitation is difficult, due to the scarcity of experiments reporting true timescales of the antiferromagnetic response. The fact that this timescale seems to be faster in $NaOsO_3$ than other Ir-based oxides could possibly point to the role played by the presence of itinerant magnetism facilitating the electron mobility and therefore the further delocalization of the magnetic moments after the fs laser excitation. However, recent experiments on FeRh, a metallic antiferromagnetic at room temperature, suggest that changes in the band structure occur

only on the order of a few hundreds of fs [69]. So it is clear that the full details of the band structure should be taken into account to obtain a quantitative description of the temporal evolution of the antiferromagnetic order parameter. In this respect, it must be also mentioned that nonequilibrium dynamic mean-field theory predicts for τ_m timescales on the order of a few fs [32]. Accordingly, to gain a deeper understanding of the interplay between the electronic structure and magnetism in oxide materials upon laser excitation, more experiments with better time resolution are required.

V. CONCLUSIONS

In summary, we have presented the results of time-resolved x-ray experiments on $NaOsO_3$, which aimed to ascertain the timescales of the melting of the antiferromagnetic structure. We have found that the magnetic order is quenched on a timescale $\tau_m \sim 71(6)$ fs, which is faster than in other perovskite compounds. These results may indicate the strong coupling between the electronic and magnetic degrees of freedom in this material. Our measurements of changes in the structural Bragg reflections show evidence of subsequent lattice dynamics extending over times of several picoseconds.

The raw data files that support this study are available via the Zenodo repository [72].

ACKNOWLEDGMENTS

We thank D. Hsieh and D. Mazzone for sharing their data, which were used to extract some of the timescales τ reported in Table II. We thank I. Lo Vecchio for sharing the $NaOsO_3$ data from Ref. [47]. We are also indebted to J. Mentink and M. Eckstein for stimulating discussions. This research work was supported from funding provided by the Swiss National Science Foundation, SNF Project No. 200021_162863, 200020-159220, and 200021-137657. This work was partially supported by NCCR Molecular Ultrafast Science and Technology (NCCR MUST No. 51NF40-183615), research instruments of the Swiss National Science Foundation (SNSF). Work in Japan was partly supported by JSPS KAKENHI Grant No. JP20H05276 and Innovative Science and Technology Initiative for Security (Grant No. JPJ004596) from Acquisition, Technology, and Logistics Agency (ATLA), Japan. The experiment at SACLA was performed with the approval of the Japan Synchrotron Radiation Research Institute (JASRI; Proposal No. 2017A8021). S.S. acknowledges ETH Zurich Post-Doctoral fellowship and Marie Curie actions for People COFUND program and the Carl Tryggers foundation with Project No. (113705531).

APPENDIX

1. Modelling of the antiferromagnetic x-ray diffracted intensity

In a static diffraction experiment, the measured intensity of a selected diffraction peak $I(q)$ is proportional to the square of the unit cell structure factor $F(q)$, with q being the momentum transfer. If the sample is excited by an ultrashort laser pulse, the expression of the structure factor needs to be modified to take into account the depth-dependent excitation profile, namely, close to the surface of the sample, the laser excitation would suppress or modify the scattering cross section, while layers further away from the surface could be unaffected, at least on very short timescales. It is customary to account for this depth dependence by splitting the sample into N layers, each at a given depth z_i. Each layer will scatter x rays differently and will contribute to the total diffracted intensity. To calculate the total diffracted intensity, two limiting cases are typically considered. In the first case, the in-plane coherence length ξ is much larger than the x-ray effective penetration depth ζ (the x-ray penetration depth ζ_X must be corrected by a geometrical factor that takes into account the scattering geometry, $\zeta \sim 3\zeta_X$ in our case). In this case, the contributions from each layer are summed in amplitude and the diffracted intensity is given by

$$I(q,t) \propto \left| \sum_{i=0}^{N} F(q,t) \right|^2. \tag{A1}$$

In the opposite case, where the penetration depth ζ is much larger than the in-plane coherence length ξ, the contributions of the different layers should be added incoherently such that the diffracted intensity is expressed as

$$I(q,t) \propto \sum_{i=0}^{N} |F(q,t)|^2. \tag{A2}$$

In our experiment, we are in an intermediate situation, where ξ and ζ are of the same order of magnitude, so it is not evident which would be the best approximation to describe the diffracted intensity. To model the experimental results, we have accordingly empirically fitted the data first with Eq. (A1) and subsequently with Eq. (A2). As shown by Fig. 3, the model based on the expression of the intensity given in Eq. (A2) reproduces well the fluence dependence of the antiferromagnetic diffracted intensity. Conversely, the model based on Eq. (A1) does not provide a reasonable description of the measured diffraction intensities. We have therefore concluded that, for our specific experimental conditions, the model based on Eq. (A2) is best suited to describe the data we have gathered on the antiferromagnetic peak.

2. Lattice dynamics

To ascertain the presence of lattice deformation due to laser induced heating or strain waves, we have performed angular scans at selected time delays on a magnetic and lattice peak. To maintain the x-ray grazing incident angle fixed during the scan, we have scanned the diffractometer angle ϕ. The results, gathered with the laser fluence of 24.05 mJ/cm^2 and normalized to 1 for the ease of comparison, are illustrated in Fig. 5(a) for the magnetic peak $(1\ \bar{5}\ 0)$ and in Fig. 5(b) for the structural peak $(1\ \bar{2}\ 2)$. The magnetic peak does not show an appreciable change of the peak position for time delays up to 10 ps. Also at time delay of several tenths of ps, where heat diffusion has occurred, the change in the peak position is tiny. Such behavior is not observed for the structural peak. As shown in Fig. 5(b), the position and shape of the $(1\ \bar{2}\ 2)$ Bragg peak changes significantly for time delays larger than 2.7 ps. Specifically, for time delay of ~ 6 ps a second peak appears at $\phi = -11.76$, indicating the presence of a laser-induced

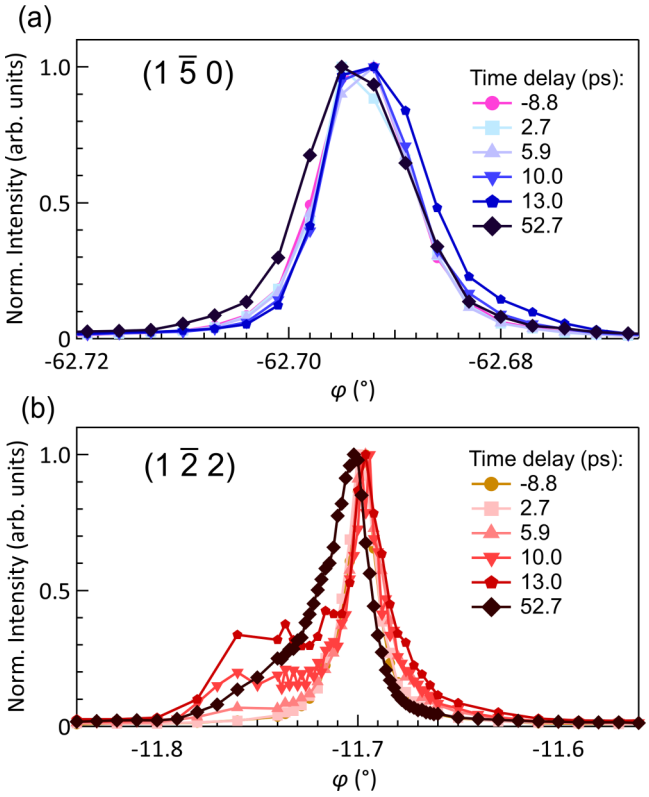

FIG. 5. Angular ϕ-scans at different time delays at the maximum excitation fluence 24.2 mJ/cm^2 for the (1 $\bar{5}$ 0) magnetic and the structural (1 $\bar{2}$ 2) Bragg peaks. The intensity for each time delay has been normalized to maximum value within each scan for the ease of comparison of the change of the peak position and peak FWHM.

heating effect. At 10 ps time delay, the presence of the second peak is more prominent and is clearly visible as a distribution of intensity between the two peaks, which we ascribe to the presence of a thermal gradient in the sample. Finally, at larger time delays, the heat has diffused from the lattice planes close to the sample surface to all the x-ray probed volume, resulting in a sizable shift of the structural Bragg peak. A thermal gradient is still present, as indicated by the larger FWHM and the asymmetric shape of the Bragg peak. The fact that the angular scans of the two peaks show such a marked difference for time delays larger than 2.7 ps can be understood as follows. The antiferromagnetic peak intensity decreases strongly as the

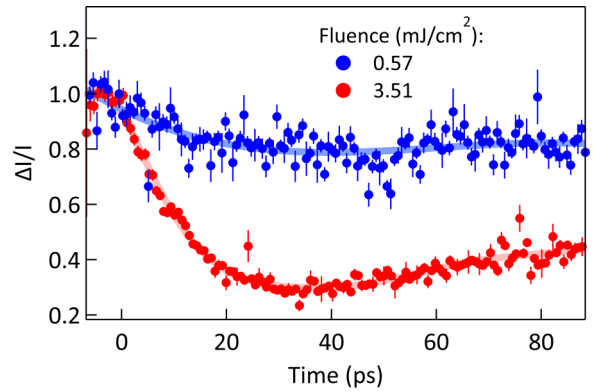

FIG. 6. Time traces of the change in intensity of the structural peak (2 $\bar{4}$ 0) measured upon photoexcitation for two different fluences.

sample temperature approaches T_N. Therefore, in the case of the magnetic peak, no second peak nor a distribution of intensity is to be expected.

As a next step, to determine the laser-induced lattice dynamics, two structural lattice peaks (1 $\bar{2}$ 2) (with no scattering contribution from the Os ion) and (2 $\bar{4}$ 0) (with a scattering contribution from the Os ion) were measured, using x rays with an incident photon energy of 10.787 keV (0.115 nm), the same used for the antiferromagnetic peak. Typically, phonon modes involving heavy ions are lower in frequency, and the laser excitation energy is transferred from electronic systems first to high energetic phonon modes. So one could expect a different time evolution for the two reflections, subsequent to the laser stimulus. The timescales of the drop in lattice peak intensities were found to be $\tau_{O,Na} \sim 11$ ps (1 $\bar{2}$ 2) and $\tau_{Os} \sim 20$ ps (see Fig. 6), so significantly slower than the observed antiferromagnetic order parameter and in a time window where coherent lattice expansion is expected to occur due to the laser heating effect in the excited sample volume. We tentatively ascribe the different dynamics observed to the different momentum transfer projection of the two reflections along the surface normal direction. Unfortunately, due to the limited amount of available measurement time, it was not possible to obtain more detailed information on the lattice deformation and a complete fluence dependence for such reflections. The observed dynamics is therefore ascribed to the expansion of the crystal lattice due to the heat deposited by the excitation laser pulses.

[1] E. Beaurepaire, J.-C. Merle, A. Daunois, and J.-Y. Bigot, Phys. Rev. Lett. **76**, 4250 (1996).

[2] M. Battiato, K. Carva, and P. M. Oppeneer, Phys. Rev. Lett. **105**, 027203 (2010).

[3] B. Y. Mueller, A. Baral, S. Vollmar, M. Cinchetti, M. Aeschlimann, H. C. Schneider, and B. Rethfeld, Phys. Rev. Lett. **111**, 167204 (2013).

[4] E. Turgut, D. Zusin, D. Legut, K. Carva, R. Knut, J. M. Shaw, C. Chen, Z. Tao, H. T. Nembach, T. J. Silva, S. Mathias, M. Aeschlimann, P. M. Oppeneer, H. C. Kapteyn, M. M. Murnane, and P. Grychtol, Phys. Rev. B **94**, 220408(R) (2016).

[5] M. Hofherr, P. Maldonado, O. Schmitt, M. Berritta, U. Bierbrauer, S. Sadashivaiah, A. J. Schellekens, B. Koopmans, D. Steil, M. Cinchetti, B. Stadtmüller, P. M. Oppeneer, S. Mathias, and M. Aeschlimann, Phys. Rev. B **96**, 100403(R) (2017).

[6] U. Ritzmann, P. Baláž, P. Maldonado, K. Carva, and P. M. Oppeneer, Phys. Rev. B **101**, 174427 (2020).

[7] C. Dornes, Y. Acremann, M. Savoini, M. Kubli, M. J. Neugebauer, E. Abreu, L. Huber, G. Lantz, C. A. F. Vaz, H. Lemke, E. M. Bothschafter, M. Porer, V. Esposito, L. Rettig, M. Buzzi, A. Alberca, Y. W. Windsor, P. Beaud, U. Staub, D. Zhu *et al.*, Nature (London) **565**, 209 (2019).

[8] C. D. Stanciu, F. Hansteen, A. V. Kimel, A. Kirilyuk, A. Tsukamoto, A. Itoh, and T. Rasing, Phys. Rev. Lett. **99**, 047601 (2007).

[9] C.-H. Lambert, S. Mangin, B. S. D. C. S. Varaprasad, Y. K. Takahashi, M. Hehn, M. Cinchetti, G. Malinowski, K. Hono, Y. Fainman, M. Aeschlimann, and E. E. Fullerton, Science **345**, 1337 (2014).

[10] C. Schubert, A. Hassdenteufel, P. Matthes, J. Schmidt, M. Helm, R. Bratschitsch, and M. Albrecht, Appl. Phys. Lett. **104**, 082406 (2014).

[11] M. S. E. Hadri, M. Hehn, G. Malinowski, and S. Mangin, J. Phys. D **50**, 133002 (2017).

[12] M. Beens, M. L. M. Lalieu, A. J. M. Deenen, R. A. Duine, and B. Koopmans, Phys. Rev. B **100**, 220409(R) (2019).

[13] A. Ciuciulkaite, K. Mishra, M. V. Moro, I.-A. Chioar, R. M. Rowan-Robinson, S. Parchenko, A. Kleibert, B. Lindgren, G. Andersson, C. S. Davies, A. Kimel, M. Berritta, P. M. Oppeneer, A. Kirilyuk, and V. Kapaklis, Phys. Rev. Materials **4**, 104418 (2020).

[14] P. Wadley, B. Howells, J. Železný, C. Andrews, V. Hills, R. P. Campion, V. Novák, K. Olejník, F. Maccherozzi, S. S. Dhesi, S. Y. Martin, T. Wagner, J. Wunderlich, F. Freimuth, Y. Mokrousov, J. Kuneš, J. S. Chauhan, M. J. Grzybowski, A. W. Rushforth, K. W. Edmonds *et al.*, Science **351**, 587 (2016).

[15] S. Y. Bodnar, L. Šmejkal, I. Turek, T. Jungwirth, O. Gomonay, J. Sinova, A. A. Sapozhnik, H.-J. Elmers, M. Kläui, and M. Jourdan, Nat. Commun. **9**, 348 (2018).

[16] M. Meinert, D. Graulich, and T. Matalla-Wagner, Phys. Rev. Applied **9**, 064040 (2018).

[17] H. Meer, F. Schreiber, C. Schmitt, R. Ramos, E. Saitoh, O. Gomonay, J. Sinova, L. Baldrati, and M. Kläui, Nano Lett. **21**, 114 (2021).

[18] X. Chen, X. Zhou, R. Cheng, C. Song, J. Zhang, Y. Wu, Y. Ba, H. Li, Y. Sun, Y. You, Y. Zhao, and F. Pan, Nat. Mater. **18**, 931 (2019).

[19] P. Němec, M. Fiebig, T. Kampfrath, and A. V. Kimel, Nat. Phys. **14**, 229 (2018).

[20] P. Werner, N. Tsuji, and M. Eckstein, Phys. Rev. B **86**, 205101 (2012).

[21] J. H. Mentink and M. Eckstein, Phys. Rev. Lett. **113**, 057201 (2014).

[22] M. Eckstein and P. Werner, Sci. Rep. **6**, 21235 (2016).

[23] A. V. Kimel, A. Kirilyuk, A. Tsvetkov, R. V. Pisarev, and T. Rasing, Nature (London) **429**, 850 (2004).

[24] A. V. Kimel, B. A. Ivanov, R. V. Pisarev, P. A. Usachev, A. Kirilyuk, and T. Rasing, Nat. Phys. **5**, 727 (2009).

[25] N. Kanda, T. Higuchi, H. Shimizu, K. Konishi, K. Yoshioka, and M. Kuwata-Gonokami, Nat. Commun. **2**, 362 (2011).

[26] T. Satoh, R. Iida, T. Higuchi, M. Fiebig, and T. Shimura, Nat. Photon. **9**, 25 (2015).

[27] A. V. Kimel, R. V. Pisarev, J. Hohlfeld, and T. Rasing, Phys. Rev. Lett. **89**, 287401 (2002).

[28] T. Kampfrath, A. Sell, G. Klatt, A. Pashkin, S. Mährlein, T. Dekorsy, M. Wolf, M. Fiebig, A. Leitenstorfer, and R. Huber, Nat. Photon. **5**, 31 (2011).

[29] K. Yamaguchi, M. Nakajima, and T. Suemoto, Phys. Rev. Lett. **105**, 237201 (2010).

[30] S. Baierl, M. Hohenleutner, T. Kampfrath, A. K. Zvezdin, A. V. Kimel, R. Huber, and R. V. Mikhaylovskiy, Nat. Photon. **10**, 715 (2016).

[31] A. D. Caviglia, M. Först, R. Scherwitzl, V. Khanna, H. Bromberger, R. Mankowsky, R. Singla, Y.-D. Chuang, W. S. Lee, O. Krupin, W. F. Schlotter, J. J. Turner, G. L. Dakovski, M. P. Minitti, J. Robinson, V. Scagnoli, S. B. Wilkins, S. A. Cavill, M. Gibert, S. Gariglio *et al.*, Phys. Rev. B **88**, 220401(R) (2013).

[32] D. Afanasiev, A. Gatilova, D. J. Groenendijk, B. A. Ivanov, M. Gibert, S. Gariglio, J. Mentink, J. Li, N. Dasari, M. Eckstein, T. Rasing, A. D. Caviglia, and A. V. Kimel, Phys. Rev. X **9**, 021020 (2019).

[33] D. G. Mazzone, D. Meyers, Y. Cao, J. G. Vale, C. D. Dashwood, Y. Shi, A. J. A. James, N. J. Robinson, J. Lin, V. Thampy, Y. Tanaka, A. S. Johnson, H. Miao, R. Wang, T. A. Assefa, J. Kim, D. Casa, R. Mankowsky, D. Zhu, R. Alonso-Mori *et al.*, Proc. Natl. Acad. Sci. USA **118**, e2103696118 (2021).

[34] V. Stoica, D. Puggioni, J. Zhang, R. Singla, G. Dakovski, G. Coslovich, M. Seaberg, M. Kareev, S. Middey, P. Kissin, R. Averitt, J. Chakhalian, H. Wen, J. Rondinelli, and J. W. Freeland, arXiv:2004.03694.

[35] J. Hohlfeld, E. Matthias, R. Knorren, and K. H. Bennemann, Phys. Rev. Lett. **78**, 4861 (1997).

[36] A. Scholl, L. Baumgarten, R. Jacquemin, and W. Eberhardt, Phys. Rev. Lett. **79**, 5146 (1997).

[37] C. Stamm, T. Kachel, N. Pontius, R. Mitzner, T. Quast, K. Holldack, S. Khan, C. Lupulescu, E. F. Aziz, M. Wietstruk, H. A. Dürr, and W. Eberhardt, Nat. Mater. **6**, 740 (2007).

[38] A. Kirilyuk, A. V. Kimel, and T. Rasing, Rev. Mod. Phys. **82**, 2731 (2010).

[39] D. Rudolf, C. La-O-Vorakiat, M. Battiato, R. Adam, J. M. Shaw, E. Turgut, P. Maldonado, S. Mathias, P. Grychtol, H. T. Nembach, T. J. Silva, M. Aeschlimann, H. C. Kapteyn, M. M. Murnane, C. M. Schneider, and P. M. Oppeneer, Nat. Commun. **3**, 1037 (2012).

[40] Y. G. Shi, Y. F. Guo, S. Yu, M. Arai, A. A. Belik, A. Sato, K. Yamaura, E. Takayama-Muromachi, H. F. Tian, H. X. Yang, J. Q. Li, T. Varga, J. F. Mitchell, and S. Okamoto, Phys. Rev. B **80**, 161104(R) (2009).

[41] S. Calder, V. O. Garlea, D. F. McMorrow, M. D. Lumsden, M. B. Stone, J. C. Lang, J.-W. Kim, J. A. Schlueter, Y. G. Shi, K. Yamaura, Y. S. Sun, Y. Tsujimoto, and A. D. Christianson, Phys. Rev. Lett. **108**, 257209 (2012).

[42] N. Gurung, N. Leo, S. P. Collins, G. Nisbet, G. Smolentsev, M. García-Fernández, K. Yamaura, L. J. Heyderman, U. Staub, Y. Joly, D. D. Khalyavin, S. W. Lovesey, and V. Scagnoli, Phys. Rev. B **98**, 115116 (2018).

[43] S. Middey, S. Debnath, P. Mahadevan, and D. D. Sarma, Phys. Rev. B **89**, 134416 (2014).

[44] B. Kim, P. Liu, Z. Ergönenc, A. Toschi, S. Khmelevskyi, and C. Franchini, Phys. Rev. B **94**, 241113 (2016).

[45] J. G. Vale, S. Calder, C. Donnerer, D. Pincini, Y. G. Shi, Y. Tsujimoto, K. Yamaura, M. M. Sala, J. van den Brink, A. D. Christianson, and D. F. McMorrow, Phys. Rev. Lett. **120**, 227203 (2018).

[46] J. G. Vale, S. Calder, C. Donnerer, D. Pincini, Y. G. Shi, Y. Tsujimoto, K. Yamaura, M. Moretti Sala, J. van den Brink, A. D. Christianson, and D. F. McMorrow, Phys. Rev. B **97**, 184429 (2018).

[47] I. L. Vecchio, A. Perucchi, P. Di Pietro, O. Limaj, U. Schade, Y. Sun, M. Arai, K. Yamaura, and S. Lupi, Sci. Rep. **3**, 2990 (2013).

[48] P. Beaud, A. Caviezel, S. O. Mariager, L. Rettig, G. Ingold, C. Dornes, S.-W. Huang, J. A. Johnson, M. Radovic, T. Huber, T. Kubacka, A. Ferrer, H. T. Lemke, M. Chollet, D. Zhu, J. M. Glownia, M. Sikorski, A. Robert, H. Wadati, M. Nakamura *et al.*, Nat. Mater. **13**, 923 (2014).

[49] T. Ishikawa, H. Aoyagi, T. Asaka, Y. Asano, N. Azumi, T. Bizen, H. Ego, K. Fukami, T. Fukui, Y. Furukawa, S. Goto, H. Hanaki, T. Hara, T. Hasegawa, T. Hatsui, A. Higashiya, T. Hirono, N. Hosoda, M. Ishii, T. Inagaki *et al.*, Nat. Photon. **6**, 540 (2012).

[50] T. Kameshima, S. Ono, T. Kudo, K. Ozaki, Y. Kirihara, K. Kobayashi, Y. Inubushi, M. Yabashi, T. Horigome, A. Holland, K. Holland, D. Burt, H. Murao, and T. Hatsui, Rev. Sci. Instrum. **85**, 033110 (2014).

[51] T. Katayama, S. Owada, T. Togashi, K. Ogawa, P. Karvinen, I. Vartiainen, A. Eronen, C. David, T. Sato, K. Nakajima, Y. Joti, H. Yumoto, H. Ohashi, and M. Yabashi, Struct. Dyn. **3**, 034301 (2016).

[52] K. Nakajima, Y. Joti, T. Katayama, S. Owada, T. Togashi, T. Abe, T. Kameshima, K. Okada, T. Sugimoto, M. Yamaga, T. Hatsui, and M. Yabashi, J. Synchrotron Radiat. **25**, 592 (2018).

[53] J. M. Glownia, J. Cryan, J. Andreasson, A. Belkacem, N. Berrah, C. I. Blaga, C. Bostedt, J. Bozek, L. F. DiMauro, L. Fang, J. Frisch, O. Gessner, M. Gühr, J. Hajdu, M. P. Hertlein, M. Hoener, G. Huang, O. Kornilov, J. P. Marangos, A. M. March *et al.*, Opt. Express **18**, 17620 (2010).

[54] I. Gierz, M. Mitrano, H. Bromberger, C. Cacho, R. Chapman, E. Springate, S. Link, U. Starke, B. Sachs, M. Eckstein, T. O. Wehling, M. I. Katsnelson, A. Lichtenstein, and A. Cavalleri, Phys. Rev. Lett. **114**, 125503 (2015).

[55] A. Caviezel, U. Staub, S. L. Johnson, S. O. Mariager, E. Möhr-Vorobeva, G. Ingold, C. J. Milne, M. Garganourakis, V. Scagnoli, S. W. Huang, Q. X. Jia, S.-W. Cheong, and P. Beaud, Phys. Rev. B **86**, 174105 (2012).

[56] Y. W. Windsor, A. Ernst, K. Kummer, K. Kliemt, C. Schüßler-Langeheine, N. Pontius, U. Staub, E. V. Chulkov, C. Krellner, D. V. Vyalikh, and L. Rettig, Commun. Phys. **3**, 139 (2020).

[57] A. Cavalleri, C. Tóth, C. W. Siders, J. A. Squier, F. Ráksi, P. Forget, and J. C. Kieffer, Phys. Rev. Lett. **87**, 237401 (2001).

[58] P. Beaud, S. L. Johnson, E. Vorobeva, U. Staub, R. A. De Souza, C. J. Milne, Q. X. Jia, and G. Ingold, Phys. Rev. Lett. **103**, 155702 (2009).

[59] S. de Jong, R. Kukreja, C. Trabant, N. Pontius, C. F. Chang, T. Kachel, M. Beye, F. Sorgenfrei, C. H. Back, B. Bräuer, W. F. Schlotter, J. J. Turner, O. Krupin, M. Doehler, D. Zhu, M. A. Hossain, A. O. Scherz, D. Fausti, F. Novelli, M. Esposito *et al.*, Nat. Mater. **12**, 882 (2013).

[60] V. Esposito, L. Rettig, E. Abreu, E. M. Bothschafter, G. Ingold, M. Kawasaki, M. Kubli, G. Lantz, M. Nakamura, J. Rittman, M. Savoini, Y. Tokura, U. Staub, S. L. Johnson, and P. Beaud, Phys. Rev. B **97**, 014312 (2018).

[61] M. Porer, L. Rettig, E. M. Bothschafter, V. Esposito, R. B. Versteeg, P. H. M. van Loosdrecht, M. Savoini, J. Rittmann, M. Kubli, G. Lantz, O. J. Schumann, A. A. Nugroho, M. Braden, G. Ingold, S. L. Johnson, P. Beaud, and U. Staub, Phys. Rev. B **101**, 075119 (2020).

[62] V. Esposito, L. Rettig, E. M. Bothschafter, Y. Deng, C. Dornes, L. Huber, T. Huber, G. Ingold, Y. Inubushi, T. Katayama, T. Kawaguchi, H. Lemke, K. Ogawa, S. Owada, M. Radovic, M. Ramakrishnan, Z. Ristic, V. Scagnoli, Y. Tanaka, T. Togashi *et al.*, Struct. Dyn. **5**, 064501 (2018).

[63] M. Burian, M. Porer, J. R. L. Mardegan, V. Esposito, S. Parchenko, B. Burganov, N. Gurung, M. Ramakrishnan, V. Scagnoli, H. Ueda, S. Francoual, F. Fabrizi, Y. Tanaka, T. Togashi, Y. Kubota, M. Yabashi, K. Rossnagel, S. L. Johnson, and U. Staub, Phys. Rev. Research **3**, 013128 (2021).

[64] M. P. M. Dean, Y. Cao, X. Liu, S. Wall, D. Zhu, R. Mankowsky, V. Thampy, X. M. Chen, J. G. Vale, D. Casa, J. Kim, A. H. Said, P. Juhas, R. Alonso-Mori, J. M. Glownia, A. Robert, J. Robinson, M. Sikorski, S. Song, M. Kozina *et al.*, Nat. Mater. **15**, 601 (2016).

[65] M. Fiebig, K. Miyano, Y. Tomioka, and Y. Tokura, Appl. Phys. B **71**, 211 (2000).

[66] T. Ogasawara, T. Kimura, T. Ishikawa, M. Kuwata-Gonokami, and Y. Tokura, Phys. Rev. B **63**, 113105 (2001).

[67] T. Ogasawara, K. Tobe, T. Kimura, H. Okamoto, and Y. Tokura, J. Phys. Soc. Jpn. **71**, 2380 (2002).

[68] P. Ruello, S. Zhang, P. Laffez, B. Perrin, and V. Gusev, Phys. Rev. B **76**, 165107 (2007).

[69] F. Pressacco, D. Sangalli, V. Uhlíř, D. Kutnyakhov, J. A. Arregi, S. Y. Agustsson, G. Brenner, H. Redlin, M. Heber, D. Vasilyev, J. Demsar, G. Schönhense, M. Gatti, A. Marini, W. Wurth, and F. Sirotti, Nat. Commun. **12**, 5088 (2021).

[70] H. Chu, L. Zhao, A. de la Torre, T. Hogan, S. D. Wilson, and D. Hsieh, Nat. Mater. **16**, 200 (2017).

[71] W. Liang, H. Hou, Y. Lin, and S.-N. Luo, J. Phys. D **52**, 075303 (2019).

[72] V. Scagnoli, "Melting of magnetic order in $NaOsO_3$ by femtosecond laser pulses", doi:10.5281/zenodo.6426862 (2022).